JOURNAL OF MATERIALS SCIENCE **35** (2000) 221–228

On the use of nanoscale indentation with the AFM in the identification of phases in blends of linear low density polyethylene and high density polyethylene

M. S. BISCHEL
Materials Science Program, University of Delaware, Newark, DE 19716 and Center for Composite Materials, University of Delaware, Newark, DE 19716
E-mail: bischel@me.udel.edu

M. R. VANLANDINGHAM
NIST, Building Materials Division, Gaithersburg, MD 20899

R. F. EDULJEE, J. W. GILLESPIE, JR., J. M. SCHULTZ
Materials Science Program, University of Delaware, Newark, DE 19716 and Center for Composite Materials, University of Delaware, Newark, DE 19716

The microstructures generated by blends of linear low density polyethylene (LLDPE) and high density polyethylene (HDPE) following isothermal crystallization from the melt have been studied using several techniques. The traditional methods of electron microscopy, wide angle X-ray scattering, and differential scanning calorimetry were used to examine the superstructures, lattice spacings, and thermal properties, respectively. In addition, nanoindentation of specific moieties within the microstructure was performed using the atomic force microscope (AFM). The indentation measurements were used to generate values for the relative elastic moduli of the crystalline features and to identify phases within the superstructures. The AFM results were compared to results obtained from the aforementioned techniques and to microhardness measurements.

1. Introduction

The morphology of a semicrystalline polymer system is affected by the manner in which the polymer is crystallized. The resulting mechanical properties of the polymer system are highly dependent on the morphology obtained. In this study, the microstructures and corresponding mechanical properties of blends of linear low density polyethylene, LLDPE, with high density polyethylene, HDPE, are investigated. These blends are gaining in commercial importance and, consequently, the morphology and mechanical properties of these systems are of interest.

The morphology of several LLDPE-HDPE blends following isothermal crystallization from the melt have been studied using several techniques. The traditional methods of scanning electron microscopy, wide angle X-ray scattering, and differential scanning calorimetry have been used to examine the superstructures, lattice spacings, and thermal properties, respectively. However, as will be discussed, these traditional methods did not unambiguously reveal the details of the mechanism for crystallization within the blend. In an attempt to identify the crystallization mechanism, the atomic force microscope, or AFM, has been used to indent specific moieties within the microstructure. Using indentation theory, these measurements can be used to generate values for the relative elastic moduli of these features and to identify phases within the superstructures. Knowledge of the changes in modulus within the superstructure can then lead to refinement of the proposed theory describing the crystallization mechanism of the blends.

Finally, because semi-crystalline polymers are a composite-like structure of amorphous and crystalline components, significant differences between the moduli of individual lamellar crystals and the modulus of the bulk material might exist. To investigate differences between local and bulk responses, the AFM indentation results have been compared to results obtained from microhardness measurements.

1.1. Nanoindentation technique

Traditionally, AFM has been used to measure the nanometer-scale topography of surfaces through direct contact between a sample surface and a probe tip mounted on the end of a cantilever microbeam. Development of the AFM's imaging capabilities has focused on the tip-sample interaction forces, leading to the utilization of the AFM as a surface force apparatus. In this

mode, termed force mode, the AFM monitors the interaction forces as a function of the perpendicular distance traversed by the tip relative to the sample surface [1, 2]. As the probe tip is lowered into contact with the sample, the tip deflection signal remains constant until the probe tip makes contact with the surface. Just before tip-sample contact is made, the probe tip can be pulled down to the surface by attractive forces. However, for probes with spring constants greater than 100 N/m, such as those used in this study, the attractive forces are not large enough to produce this effect [3]. Decreasing the tip height further causes the cantilever to deflect in the opposite direction, resulting in an increased tip deflection signal. During unloading, the piezo actuator retracts and the cantilever deflection reduces until the tip separates from the sample surface. Often, however, the tip adheres to the surface, causing a further decrease in the tip deflection signal until the tip jumps out of contact.

To extract the nanoscale response of the material to indentation, the tip-sample interaction is modeled as two springs in series, as shown in Fig. 1. After contact is made between the probe tip and the sample surface, piezo displacement results in both probe tip deflection and sample indentation, the amounts of which depend on the relative stiffnesses of the sample and the cantilever probe [4, 5]. Thus, the amount of penetration of the tip into the sample, Δz_i, is just the difference between the piezo motion, Δz_p, and the deflection of the probe tip, Δz_t. Also, Δz_t is directly proportional to the probe force, P, through the probe spring constant k_c. For the AFM system used in this study, a factor equal to cos (10°) is necessary to account for the 10° angle of the probe to the horizontal, as indicated in Fig. 1. For a sample which is infinitely stiff with respect to the probe, no indentation will occur, and the slope of the contact portion of the force curve will reach a maximum value. Such a sample is needed to calibrate the system and minimize experimental error [4, 6, 7].

Assuming the unloading response consists of pure elastic recovery, the unloading curve can be fit to a power law relationship between indentation depth and load which has the form [8, 9]

$$P = \frac{\xi E}{(1-\nu^2)}(\Delta z_i)^m \tag{1}$$

where ξ is a constant which depends on the contact radius, r, E and ν are the sample elastic modulus and Poisson's ratio, respectively, and m is a power law exponent.

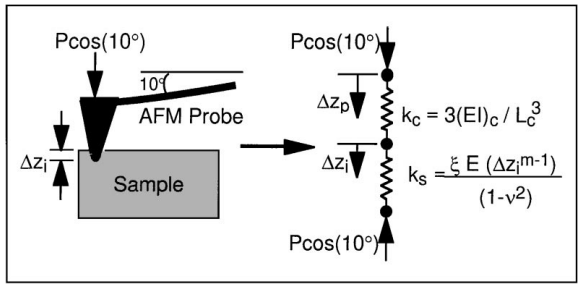

Figure 1 Spring model of the tip-sample interaction during the unloading portion of an indentation test with the AFM.

Thus, measurements obtained from the indentation response can be used to calculate the elastic modulus of the feature indented [1–13]. To obtain exact modulus values, however, an independent assessment of the contact radius as a function of penetration depth is required. If the same force range is used to indent two materials, if the resulting power law exponents, m, are the same, and if equivalent Poisson's ratios for the two materials is assumed, then the indentation response of material 1 to that of material 2 can be related as follows [6, 7]:

$$\frac{(\Delta z_i)_2}{(\Delta z_i)_1} = \frac{r_1 E_1}{r_2 E_2} \tag{2}$$

Here, the Δz_i values used are normally taken as the maximum recovered displacements over the entire unloading curve. If the contact radii can be related, for example by using the relative sizes of the plastic indents, relative values of elastic moduli between samples or between areas of a single sample can then be calculated.

This technique has been validated in studies of polyurethanes and epoxies [6, 7]. In this work, it will be used to identify phases within polymer blends and to quantity variations in modulus within a crystalline superstructure.

1.2. Microhardness

Microhardness measurements provide a relatively simple means for determining mechanical properties of small samples. Although microhardness is typically used to analyze brittle materials [14], this technique has recently become popular for the evaluation of polymeric systems [15–23]. Further, most of the deformation in polymers during hardness testing is plastic in nature [19].

For Vickers microhardness testing, a square-based pyramid with included angles between opposite faces of $\theta = 136°$ [21] is used. The hardness, H, which is equivalent to the indentation pressure, is a function of the applied force, P, in newtons and the area of the plastic impression in mm^2:

$$H = \frac{2P\sin(\theta/2)}{d^2} \tag{3}$$

where d is the mean diagonal length of the impression [22]. A power law relationship between H and elastic modulus, E, has been suggested for semicrystalline polymers [22]:

$$H = aE^b \tag{4}$$

Because of the recent use of microhardness testing and, therefore, lack of microhardness data for polymers, accurate values for the power law parameters a and b are not available. However, a microhardness study including commercial grades of unetched HDPE and LLDPE has reported linear decreases in indentation recovery with both increasing modulus and increasing microhardness, yielding a linear relationship between microhardness and modulus [23]. Therefore, in this study, the

following equation will be used:

$$H = \beta E \tag{5}$$

Thus, relative hardness values can be used as relative modulus values.

2. Experimental

2.1. Materials

The neat polymers used in this study are a commercial linear low density polyethylene, LLDPE, Exxon 3025-Exact, and a commercially obtained narrow fraction of high density polyethylene, HDPE. The important characteristics of both materials are given in Table I.

2.2. Methods

Blends of the neat polymers were made by dissolving the components in boiling xylene and then precipitating in methanol [24, 25]. Two blends were examined; the first blend is a one-to-one ratio of HDPE to LLDPE and will be referred to as the 50/50 blend; the second blend is a three-to-one ratio of HDPE to LLDPE and will be referred to as the 75/25 blend. Isothermal crystallization was performed in a Mettler FP82 hot stage for times sufficiently long to allow for total crystallization. For all samples used in this study, the crystallization temperature was $105\,^{\circ}\mathrm{C} \pm 1.1\,^{\circ}\mathrm{C}$. This crystallization temperature is several degrees less than the maximum, practical crystallization temperature of the LLDPE, and is well below that of the HDPE.

Potassium permanganate-based etchants were used to reveal the microstructures of the neat polymers and blends [24, 26]. For the blends, a two-step etching process was developed; the LLDPE structure is revealed by the first step, and the HDPE structure is revealed by the second [24, 27]. The microstructures were then examined using scanning electron microscopy, SEM, and atomic force microscopy. Also, lattice parameters were determined from wide angle X-ray scattering measurements, WAXS. The WAXS data was obtained using an INEL Curved Position Sensor detector CPS-120, an accelerating voltage of 30 kV, and a CuK_{α} source [24].

Thermal properties, including melting behaviors, were measured using a Perkin Elmer DSC-7 with a melting rate of $30\,^{\circ}\mathrm{C}$/min [24]. Microhardness measurements were made on unetched samples using a Buehler Micromet II. For these studies, a Vickers indenter was used with a load of 25 g [24].

A Digital Instruments D3000 scanning probe microscope was used to produce force curves from the interaction of a silicon single-beam cantilever probe with both of the etched homopolymers and the etched blends. Etched samples were used so that specific microstructural features could be examined.

The probe, shown schematically in Fig. 1, was a cantilever microbeam with a sharp tip attached at one end. The approximate cantilever dimensions, as supplied by the manufacturer were as follows: width $= 72\,\mu$m, length $= 124\,\mu$m, and thickness $= 7.1\,\mu$m. The tip geometry, also supplied by the manufacturer, was similar to that of a triangular pyramid with tip half angles of 10° to 25°. The approximate tip height $= 10$–$15\,\mu$m, while the tip radius $= 5$–10 nm, thus yielding a sufficiently sharp tip for probing local responses to indentation. The spring constant of the probe was estimated to be 250 ± 50 N/m.

All indentations were made using a displacement rate of $4\,\mu$m/s to avoid effects of rate-dependent deformation and piezo hysteresis. Also, compensation for lateral tip motion was used as described elsewhere [7]. A sapphire sample, $E = 470$ GPa [4], has been used as an "infinitely stiff" material for system calibration.

TABLE I Characteristics of neat polymers

Property	LLDPE	HDPE
Peak M_W	59,826	27,700
Polydispersity	2.04	1.99
Theoretical value of Elastic modulus	0.1 GPa (provided by Exxon)	5–10 GPa (from reference 28)
Branch content per 1000 C	21	<1

3. Results and discussion

3.1. Morphology

Microscopy results indicate that, at a crystallization temperature of $105\,^{\circ}\mathrm{C}$, the LLDPE copolymer forms banded spherulites with an average radius of $21 \pm 6\,\mu$m, while the HDPE forms axialites with a dimension of $4.5 \pm 0.5\,\mu$m in the elongated direction. The microstructure of the 50/50 blend consists of banded spherulites, which have an average radius of $16 \pm 4\,\mu$m, with a large axialite at the center of each banded spherulite that is revealed during the HDPE etch. This microstructure is shown in Fig. 2a. The 75/25 blend forms an axialitic structure with an average length of $16 \pm 3\,\mu$m, as shown in Fig. 2b. From the micrographs, however, determination of the distribution of LLDPE and HDPE within the blend superstructures is not possible.

Two materials-related questions arise with regard to the method of crystallization in the 50/50 blend. These questions are related to the fact that the neat HDPE crystallizes much more rapidly than does the neat LLDPE [24]. First, is the central axialite created by the initial crystallization of neat HDPE, with the remaining banded spherulite composed of LLDPE-rich material? Second, does the banding result in a radially periodic modulation in composition? One period of such a composition modulation would be due to the buildup of LLDPE at the interface, choking off the rapid growth of the HDPE-rich material, leading to the crystallization of that LLDPE-rich pool. During the next period, HDPE-rich material would crystallize from a melt which is now depleted of LLDPE. These questions can be addressed using the nanoindentation results.

3.2. Nanoindentation

Nanoindentation was performed on etched samples using the AFM. First, the AFM was used in TappingMode™ to produce images of the crystalline microstructures. Specific features were then indented and subsequently imaged, again in TappingMode™, to

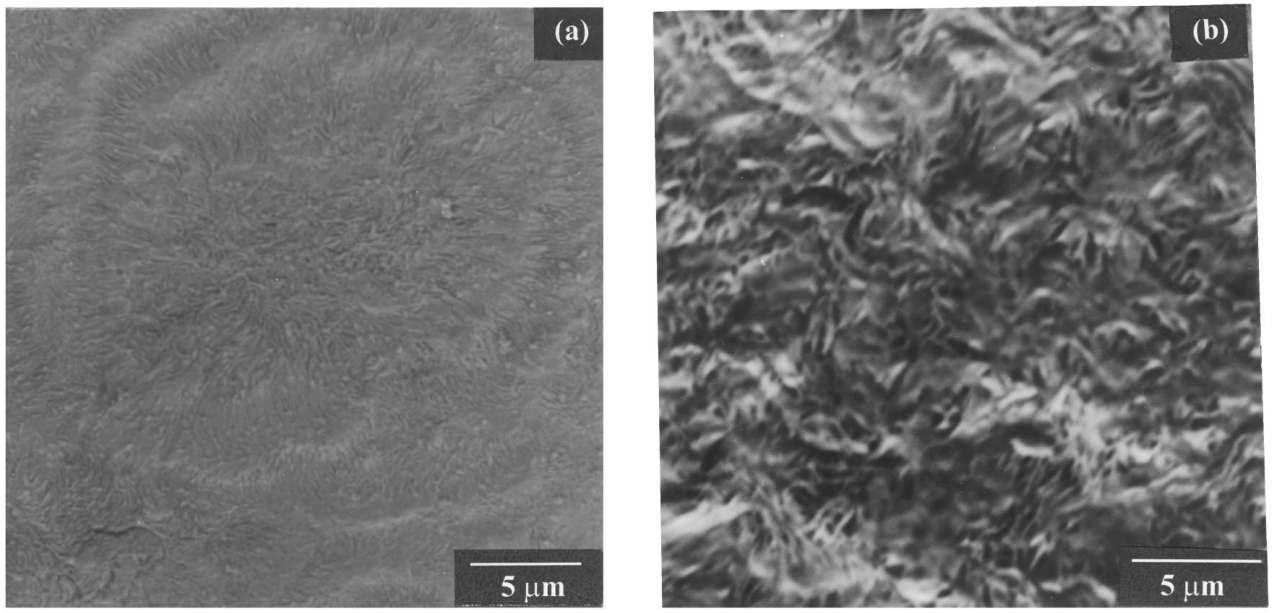

Figure 2 Micrographs of (a) 50/50 blend and (b) 75/25 blend. Samples are etched, and sputtered with Au; viewed in SEM.

reveal the size of the plastic deformation produced and the relative positions of the indentations. Triangular impressions were produced in the samples due to the triangular cross-section of the probe tip. The distance from the apex to the base of each triangular impression was taken as a measurement of the plastic indent size. The force curves produced from each indentation were then analyzed as outlined in the previous section. Note that the etching process can affect the material response to indentation, as etching generally removes amorphous components within the superstructure [26] and tends to chemically harden the sample [16]. However, because all samples used for the nanoindentation tests were etched, the quantitative effect on the relative responses should not be significant.

3.2.1. Comparison of LLDPE and HDPE

For the etched LLDPE sample, indentations were made in the center of a banded spherulite, while for the HDPE sample, indents were made across the lamellar arms of the HDPE axialites. Eight indents were made on each sample. The LLDPE is observed to be much more compliant and more easily deformed plastically than the HDPE sample. Load-unload curves for both materials are shown in Fig. 3. For the two unloading curves, power law fits using Equation 1 yield power law exponents of $m = 1.9$ for both, indicating a similar unloading geometry [9]. However, the elastic indentation displacement for the LLDPE is approximately 15 times larger than that of the HDPE for the same maximum load. This result indicates a much lower modulus for the LLDPE as compared to the HDPE. Also, the amount of hysteresis between the loading and unloading curves, which is a function of plastic deformation and tip-sample adhesion, is larger for the LLDPE sample. This result correlates with the observed plastic indent sizes, which range from 250–290 nm for the LLDPE and from 60–90 nm for the HDPE. Using Equation 2 and assuming the relative indent sizes are an indication of relative contact radii, the modulus of the HDPE axialite is predicted to be approximately 50 to 60 times greater than the modulus of the LLDPE spherulite. This result is consistent with values found in the literature ($E_{\mathrm{LLDPE}} = 0.1$ GPa; $E_{\mathrm{HDPE}} = 5$–10 GPa [28]).

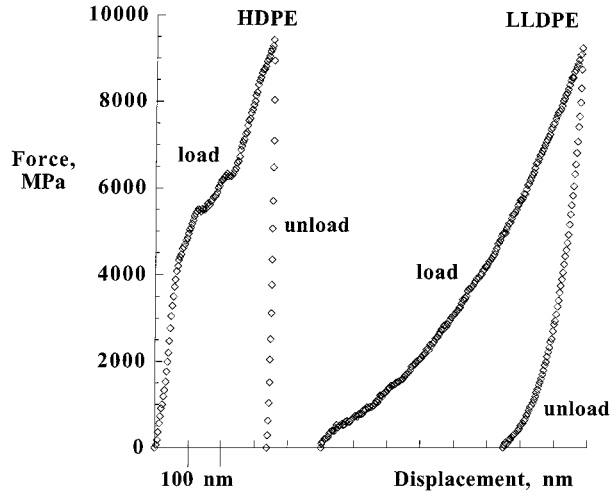

Figure 3 Load-unload curves for LLDPE and HDPE indented with a 250 N/m probe. Both unloading curves are characterized by a power law exponent $m = 1.9$.

The accuracy of this relative modulus value, however, is questionable due to the differences in the loading curves. For the HDPE, the slope of the loading curve decreases at several points with increasing load, while the slope of the LLDPE loading curve increases continuously with load. This observation might be an indication of two different deformation processes. For the HDPE, the initial part of the loading curve most likely consists of both elastic and plastic deformation. As tip penetration depth and plastic indent size increase, the contact radius increases, increasing the contact stiffness, S, defined by

$$S = \frac{2rE}{(1 - \nu^2)} \tag{6}$$

As S becomes much larger than the probe spring constant, k_c, elastic deformation will not be possible, and

thus increasing the force will produce only plastic deformation. For the HDPE, which has an estimated modulus value of 5–10 GPa, S will exceed k_c early in the loading process, yielding extremely small values of Δz_i, ranging from 6–9 nm. Therefore, the initially steep slope is most likely indicative of elastic plus plastic deformation; as the relative amount of elastic deformation decreases, the slope of the loading curve decreases. For the LLDPE, which has an estimated modulus of 0.1 GPa, $S < k_c$ for the entire load-unload curve and large values of Δz_i, 110–120 nm, are obtained. The increase in slope with increasing load is characteristic of a continuous increase in contact radius with penetration depth [9, 29]. Relative comparisons of materials characteristics, and in particular relative modulus values, might not be accurate because the state of deformation for the two materials was reached through entirely different pathways. In general, this technique is difficult to use to quantitatively evaluate materials with large modulus differences [7].

3.2.2. Comparison of 50/50 and 75/25 blends

For the 50/50 blend, indentations were made on the axialitic-shaped center of the banded spherulite, and in the peaks and valleys of the bands. At least ten indentation measurements were made in each region. For the 75/25 blend, ten indentations were made across the lamellar arms. Representative load-displacement curves for the two blends are shown in Fig. 4. The load-unload curves have similar shapes, indicating similar deformation paths, and the plastic indent sizes as well as the load-unload hysteresis values are only slightly larger for the 50/50 blend. Elastically, the 75/25 blend is significantly stiffer with Δz_i values of the order of 11 ± 3 nm for values of the power law exponent, m, between 1.8 and 2.0. The Δz_i values for the 50/50 blend are approximately 25 ± 4 nm in valleys, 35 ± 7 nm along peaks, and 28 ± 5 nm on the center axialite for m values similar to those of the 75/25 blend. Using the Δz_i values for the 50/50 center axialite, which nearly

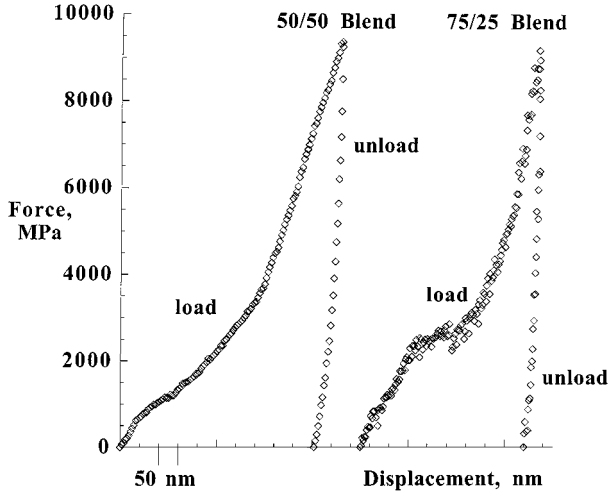

Figure 4 Load-unload curves for 50/50 and 75/25 blends indented with a 250 N/m probe. Both unloading curves are characterized by a power law exponent $m = 1.9$.

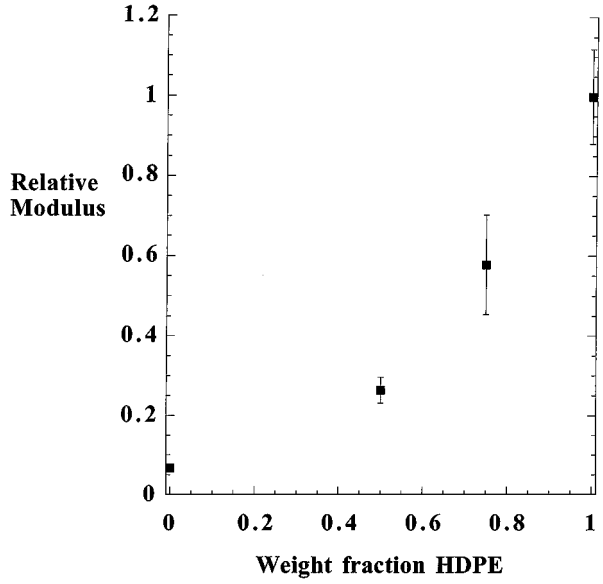

Figure 5 Relative elastic modulus as a function of HDPE content. Values are calculated from indentation responses measured using the AFM.

equals the average of the responses from the peaks and valleys, and assuming equal contact radius values, the modulus ratio for the 75/25 blend with respect to the 50/50 blend calculated to be approximately 2.5.

Comparing the responses of the blends to that of the HDPE and LLDPE samples, the blends generally behave more like the HDPE. In fact, compared to the HDPE, the 75/25 blend has similar load-unload hysteresis values, approximately 170 nm; slightly larger elastic indentation values, 11 ± 3 nm vs 7.5 ± 2 nm; and slightly larger plastic indent sizes, 95 ± 15 nm vs 75 ± 15 nm. Using the relative plastic indent sizes as an indication of relative contact radii, values for the relative elastic moduli for the blends and the neat polymers can be calculated using Equation 2. The results are shown in Fig. 5 as a function of HDPE content, with the values for the LLDPE and the blends normalized by that of the HDPE. Clearly, the moduli for the two neat polymers are distinctly different from those of the blends. Further, the relative modulus increases monotonically with increasing HDPE content. This result indicates that the center of the axialite in the 50/50 blend is not HDPE; likewise, the axialites observed in the 75/25 blend are not composed of HDPE. Therefore, the nanoindentation results indicate that the superstructures of these blends are composed of co-crystals of the LLDPE and HDPE. No phase segregation on a scale larger than that of the nanoindention can be observed within individual banded spherulites or axialites.

3.2.3. Relative modulus versus radial position in the 50/50 blend

For the 50/50 blend, the relative modulus as a function of radial position across the banded spherulite was also examined. Two sets of indentations were made across a spherulite beginning in the center and stepping radially outward in increments of 500 nm. These sets of indents are in addition to the two sets taken along a single peak and through a single valley, respectively, as commented

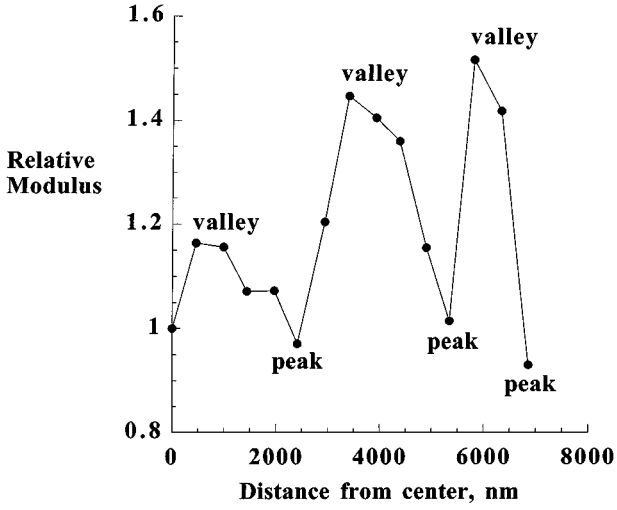

Figure 6 Relative elastic modulus, measured using the AFM, as a function of radial distance across a spherulite in the 50/50 blend.

upon in the previous subsection; the results are similar. Assuming equal contact radii, relative modulus values can be calculated; the results are plotted as a function of radial distance from the center of the spherulite in Fig. 6. The positions of the peaks and valleys are indicated. The valleys are thus stiffer than the peaks, while intermediate regions have moduli that fall between those of the peaks and valleys.

These results could be influenced by the changes in topography across the spherulite. However, the amounts of load-unload hysteresis and the shapes of the load-unload curves are similar and the plastic indent size is sufficiently small compared to the distances between peaks and valleys. Thus, the topographic differences do not significantly affect the indentation results. More likely, the orientation of the lamellar crystals within the peaks is different than in the valleys, such that the resistance to deformation is higher in the valleys than on the peaks [21]. Such a change in orientation between the peak and valley of a single band is consistent with the geometry required for banded spherulites [30–35].

3.3. Microhardness

Microhardness measurements were made on etched and unetched samples of the two blends and the two neat polymers. The geometry of the microhardness tests was such that each indentation covers several different spherulites and/or axialites. Thus, the results should be representative of a bulk material response, as opposed to the local responses measured in the nanoindentation tests. The microhardness values obtained for the unetched samples are plotted as a function of HDPE content in Fig. 7a. The corresponding values of elastic modulus have been calculated using Equation 5 and normalized by the value for the HDPE, and are shown in Fig. 7b. Note that the results for the etched samples are similar to the results obtained using unetched samples, indicating that the bulk response was not significantly effected by the etching process.

Comparing Fig. 7b to Fig. 5, both the AFM indentation results and the microhardness results indicate that the blends have significantly different mechanical properties than the neat polymers. However, the microhardness results of the two blends are indistinguishable, while the AFM indentation results show a distinct difference in response. Also, the modulus of the HDPE is only a factor of 5 larger than that of the LLDPE using the microhardness results. This result correlates well with similar microhardness testing of unetched HDPE and LLDPE [22]. In contrast, the AFM technique predicts a much larger modulus ratio of approximately 50 between the HDPE and LLDPE crystalline regions. Therefore, for this set of polymeric materials, the AFM indentation technique is much more sensitive to small, local differences in modulus than is microhardness testing.

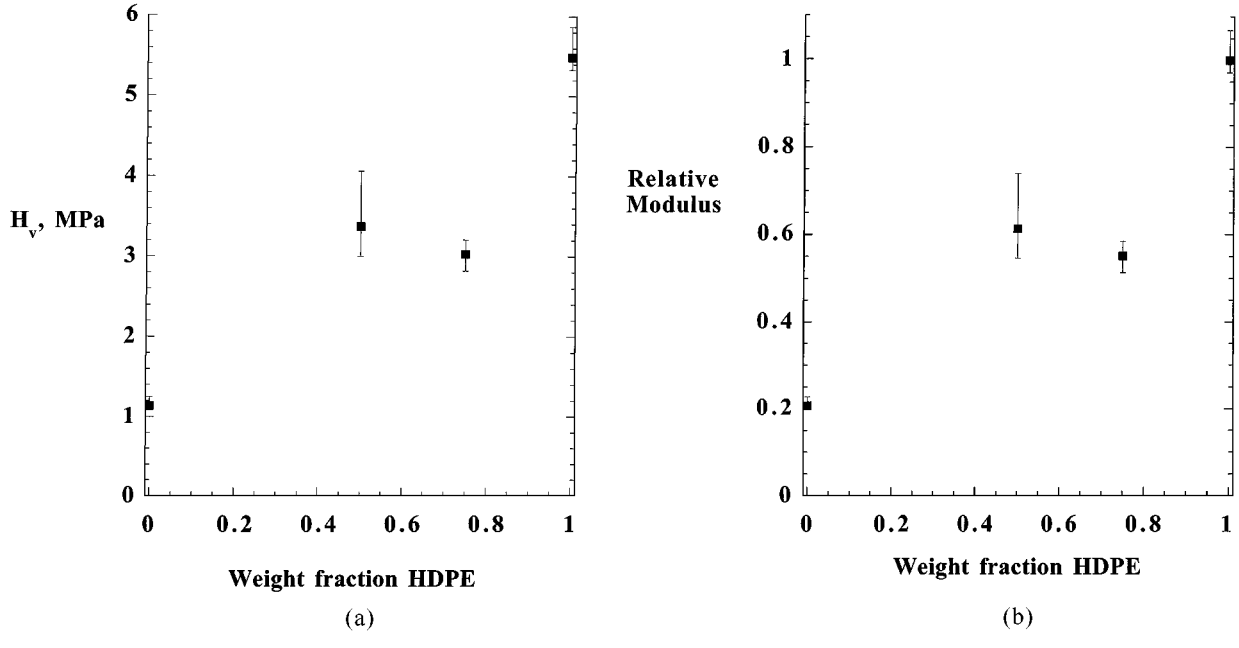

Figure 7 (a) Microhardness, H_v, and (b) relative modulus calculated using microhardness results, as functions of HDPE content.

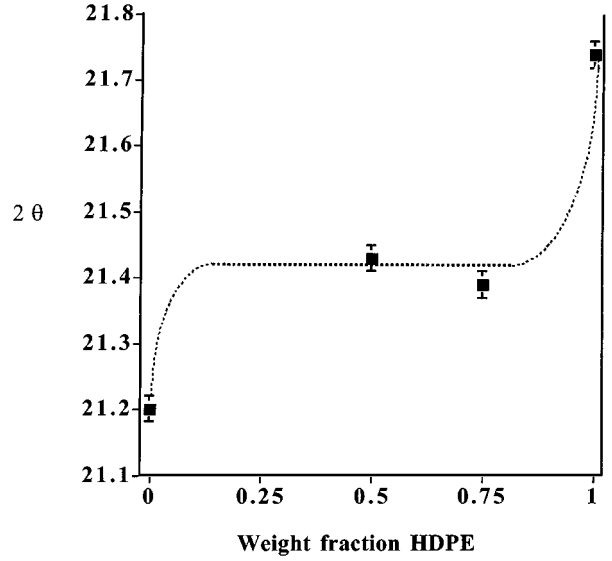

Figure 8 WAXS data for the (1 1 0) peak, as a function of HDPE content.

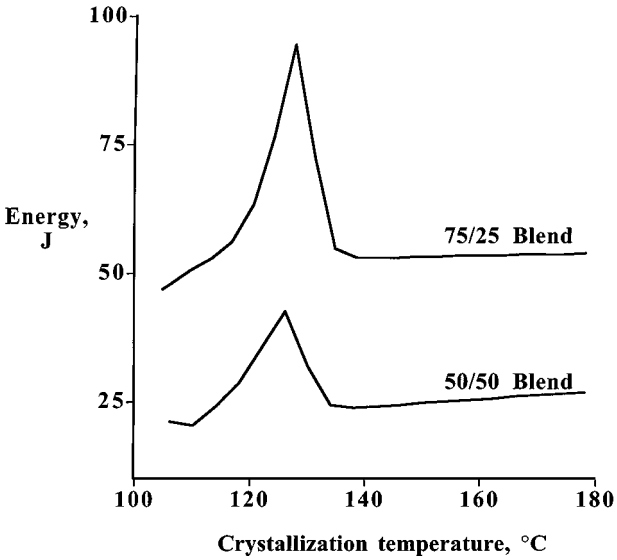

Figure 9 DSC melting curves for the 50/50 and 75/25 blends, following isothermal crystallization at 105 °C.

3.4. Other results

The results of the nanoindentation measurements which suggest co-crystallization within the LLDPE/HDPE blends are substantiated by results from other techniques. The results of WAXS measurements for the (110) reflections, shown in Fig. 8, indicate co-crystallization within the blends. The peak positions of the blends are equal, within experimental error, but are substantially different from those of the component polymers. Also, the results of DSC melting studies, shown in Fig. 9, indicate that co-crystallization has occurred within the blends: for both the 50/50 and 75/25 blends, following isothermal crystallization at 105 °C, a single melting peak is observed at approximately 127 °C. The melting peaks for the neat LLDPE and HDPE occur at approximately 110 and 132 °C, respectively.

4. Conclusions

Blends of LLDPE and HDPE have been studied using the atomic force microscope as a nanoscale indentation system. From the results, the relative modulus of the crystalline regions is observed to increase with increasing HDPE content. For the two neat polymers, the loading curves exhibit distinctly different behaviors due to the difference in the relative stiffness between the sample and the AFM probe. Although this difference adds a degree of uncertainty to the relative modulus calculations, the ratio of elastic modulus between the HDPE and LLDPE crystalline regions is an order of magnitude larger than that estimated from microindentation measurements. Further, the microindentation results showed no difference between the two blends, while the nanoindentation results revealed a modulus ratio of approximately 2.5 between the 75/25 blend and the 50/50 blend. These differences are representative of differences between local response, measured by nanoindentation, and bulk response, measured by microhardness. Also, using nanoindentation, relative modulus values across a spherulite of the 50/50 blend have been measured. Small modulus changes are observed, indicating a change in crystalline orientation with each band. These results indicate that the AFM indentation technique is more sensitive to small differences in stiffness than traditional microindentation techniques, and can be used to probe much smaller regions.

For blends examined in this study, nanoindentation has been used along with microindentation, WAXS, and DSC to confirm the existence of co-crystals within the superstructures. However, this technique could potentially be used even more effectively in blend systems in which the polymers are not miscible or for which the neat polymers have similar microstructures that cannot be distinguished using microscopy techniques.

Acknowledgement

The authors would like to thank Dr. W. K. Wong of Exxon International for providing the LLDPE material, Glover A. Jones of the DuPont Experimental Station for providing access to the High-Low Temperature In Situ X-ray Diffraction Laboratory, and Dr. Betsy McCord of the DuPont Experimental Station for determining the branch content of the LLDPE.

References

1. N. A. BURNHAM, R. J. COLTON and H. M. POLLOCK, *J. Vac. Sci. Technol. A* **9** (1991) 2548.
2. S. M. HUES, R. J. COLTON, E. MEYER and H.-J. GUNTHERODT, *MRS Bull.* **18** (1993) 41.
3. S. P. JARVIS, T. P. WEIHS, A. ORAL and J. B. PETHICA in "Thin Films: Stresses and Mechanical Properties IV," Vol. 308, San Francisco, April 1993, edited by P. H. Townsend (Materials Research Society, Pittsburgh, PA, 1993) p. 127.
4. P. MAIVALD, H. J. BUTT, S. A. C. GOULD, C. B. PRATER, B. DRAKE, J. A. GURLEY, V. B. ELINGS and P. K. HANSMA, *Nanotechnol.* **2** (1991) 103.
5. A. L. WEISENHORN, M. KHORSANDI, S. KANSAS, V. GOTZOS and H.-J. BUTT, *Nanotechnol.* **4** (1993)106.
6. M. R. VANLANDINGHAM, S. H. MCKNIGHT, G. R. PALMESE, R. F. EDULJEE, J. W. GILLESPIE, JR., and R. L. MCCULLOUGH in "Structure and Evolution of Surfaces," Vol. 458, Boston, December 1996, edited by R. C. Cammarata (Materials Research Society, Pittsburgh, PA, 1997) p. 313.
7. M. R. VANLANDINGHAM, S. H. MCKNIGHT, G. R. PALMESE, J. R. ELINGS, X. HUANG, T. A. BOGETTI,

R. F. EDULJEE and J. W. GILLESPIE, JR., *J. Adhesion* **64** (1997) 31.
8. I. N. SNEDDON, *Int. J. Engng. Sci.* **3** (1965) 47.
9. A. BOLSHAKOV, W. C. OLIVER and G. M. PHARR in "Thin Films: Stresses and Mechanical Properties V," Vol. 356, Boston, December 1994, edited by S. P. Baker (Materials Research Society, Pittsburgh, PA, 1995) p. 675.
10. G. M. PHARR, W. C. OLIVER and F. R. BROTZEN, *J. Mater. Res.* **7** (1992) 613.
11. A. C. M. YANG, M. S. KUNZ and T. W. WU in "Thin Films: Stresses and Mechanical Properties IV," Vol. 308, San Francisco, April 1993, edited by P. H. Townsend (Materials Research Society, Pittsburgh, PA, 1993) p. 511.
12. N. A. BURNHAM and R. J. COLTON, *J. Vac. Sci. Technol. A* **7** (1989) 2906.
13. S. M. HUES, C. F. DRAPER and R. J. COLTON, *J. Vac. Sci. Technol. B* **12** (1194) 2211.
14. D. B. MARSHALL and B. R. LAWN, in "Microindentation Techniques in Materials Science and Engineering," ASTM Special Technical Publication 889, edited by P. J. Blau and B. R. Lawn (American Society for Testing and Materials, Philadelphia, 1985) p. 26.
15. H. G. FRITZ, Q. CAI, M. E. CAGIAO, L. GIRI and F. J. BALTÁ-CALLEJA, *J. Mater. Sci.* **30** (1995) 3300.
16. F. J. BALTÁ-CALLEJA, J. MARTINEZ-SALAZAR and D. R. RUEDA, "Encyclopedia of Polymer Science and Engineering," vol. 7 (Wiley Interscience, New York, 1987) p. 328.
17. C. SANTA CRUZ, F. J. BALTÁ-CALLEJA, H. G. ZACHMANN, N. STRIBECK and T. ASANO, *J. Polym. Sci. B* **29** (1991) 819.
18. F. J. BALTÁ-CALLEJA, C. SANTA CRUZ, R. K. BAYER and H. G. KILIAN, *Colloid Polym. Sci.* **268** (1990) 440.
19. F. J. BALTÁ-CALLEJA, C. SANTA CRUZ, C. SAWATARI and T. ASANO, *Macromol.* **23** (1990) 5352.
20. Y. DESLANDES and E. ALVA ROSA, *Polym. Commun.* **31** (1990) 269.2
21. F. J. BALTÁ-CALLEJA, *Adv. Polym. Sci.* **66** (1985) 117.
22. V. LORENZO, J. M. PEREÑA and J. G. FATOU, *J. Mater. Sci. Lett.* **8** (1989) 1455.
23. V. LORENZO, J. M. PEREÑA, J. G. FATOU, J. A. MENDEZ-MORALES and J. A. AZNAREZ, *J. Mater. Sci.* **23** (1988) 3168.
24. M. S. BISCHEL, PhD Dissertation, University of Delaware, 1997.
25. K. TASHIRO, R. S. STEIN and S. L. HSU, *Macromol.* **25** (1992) 1801.
26. K. L. NAYLOR and P. J. PHILLIPS, *J. Polym. Sci. B* **21** (1983) 2011.
27. M. S. BISCHEL and J. M. SCHULTZ, in Proceedings of Microscopy and Microanalysis '96, Minneapolis, August 1996 (Microscopy Society of America, Pocasset, MA, 1996) p. 22.
28. J. BRANDRUP and E. H. IMMERGUT (eds.) "Polymer Handbook" (Wiley-Interscience, New York, 1975).
29. H. BENABDALLAH and J.-P. CHALIFOUX, *Polym. Testing* **13** (1994) 377.
30. P. H. GEIL, "Polymer Single Crystals" (Interscience Publishers, New York, 1963).
31. H. D. KEITH and F. J. PADDEN, JR., *J. Polym. Sci.* **39** (1959) 101.
32. A. KELLER, *ibid*. **39** (1959) 151.
33. D. C. BASSETT and A. M. HODGE, *Polym.* **19** (1978) 469.
34. Y. FUJIWARA, *J. Appl. Polym. Phys.* **4** (1960) 10.
35. D. C. BASSETT, in "Crystallization of Polymers," edited by M. Dosiere (Kluwer Academic Publishers, The Netherlands, 1993) p. 107.

Received 1 May 1997
and accepted 18 June 1999